HHS Public Access

Author manuscript

Nat Immunol. Author manuscript; available in PMC 2018 February 28.

Published in final edited form as:

Nat Immunol. 2017 October ; 18(10): 1128–1138. doi:10.1038/ni.3832.

Two amino acid mutation disrupts RORγt function in Th17 differentiation but not thymocyte development

Zhiheng He[1,#], **Jian Ma**[1,#], **Ruiqing Wang**[1,2], **Jing Zhang**[1,2], **Zhaofeng Huang**[3], **Fei Wang**[1], **Subha Sen**[1], **Ellen V. Rothenberg**[4], and **Zuoming Sun**[1,*]

[1]Division of Molecular Immunology, Beckman Research Institute of City of Hope, Duarte, CA, United States

[2]Irell & Manella Graduate School of Biological Sciences, City of Hope, Duarte, CA, United States

[3]Zhongshan School of Medicine, Sun Yat-sen University, Guangzhou, Guangdong, P.R. China

[4]Division of Biology & Biological Engineering, California Institute of Technology, Pasadena, California, USA

Abstract

RORγt regulates T_H17 differentiation, thymic T cell development and lymph node genesis. Although elimination of RORγt prevents T_H17-mediated experimental autoimmune encephalomyelitis (EAE), it also disrupts thymocyte development, which could lead to lethal thymic lymphoma. Here we identified two amino acid mutations in RORγt ($ROR\gamma t^M$) that preferentially disrupted T_H17 differentiation but not thymocyte development. Mice expressing $RORγt^M$ were resistant to EAE associated with defective T_H17 differentiation, but maintained normal thymocyte development and lymph node genesis, except for Peyer's patches. $ROR\gamma t^M$ showed reduced ubiquitination at K69 that is selectively required for T_H17 differentiation but not T cell development. This study will inform the development of treatments that selectively target T_H17-mediated autoimmunity, but do not affect thymocyte development and induce lymphoma.

The transcription factor RORγt, encoded by the gene *rorc2,* instructs the differentiation of T helper 17 (T_H17) cells. Activation of naïve T cells in the presence of TGF-β and interleukin 6 (IL-6) is sufficient to up-regulate RORγt and induce differentiation into T_H17 cells [1]. T_H17 cells produce the effector cytokines including IL-17 to mediate the pathological inflammation responsible for autoimmunity such as psoriasis and multiple sclerosis [2, 3, 4]. In

*Corresponding author: Zuoming Sun, Division of Molecular Immunology, Beckman Research Institute of City of Hope, 1500 East Duarte Road, Duarte, CA 91010, Phone: 626-256-4673, Fax: 626-256-6415, zsun@coh.org.

#These authors contributed equally

Materials & Correspondence. Correspondence to: Zuoming Sun.

Author contributions. Z. Sun and He, Z. conceived the study. He, Z., Ma, J., Wang, R., Huang, Z., Sen, S., Zhang, J., and Wang, F. carried out the experiments. Z. Sun and He, Z. wrote the manuscript. E. R. instructed and provided critical reagents for *in vitro* thymocyte development experiments. All the authors reviewed and edited the manuscript.

Competing financial interests. The authors declare no competing financial interests.

RNA-seq and ChIP-seq data access code is SUB2581283

The data that support the findings of this study are available from the corresponding author upon request.

addition, during thymocyte development, RORγt is up-regulated at the $CD4^+CD8^+$ (DP) stage to enhance their survival by up-regulating anti-apoptotic Bcl-x_L [5]. *RORγt*$^{-/-}$ mice develop lethal thymic lymphomas likely resulting from abnormal thymocyte development [6]. *RORγt*$^{-/-}$ mice also lack all lymph nodes, including gut-associated mesenteric lymph nodes and Peyer's patches [5, 7], due to a requirement of RORγt for the development of lymphoid tissue inducer (LTi) cells, the progenitors for lymph node genesis [5, 8, 9]. The mechanisms that distinguish the functions of RORγt in T_H17 differentiation in the peripheral immune system and thymocyte development in the central immune system remain unknown. Dissecting these functions is critical for understanding how one central transcription factor regulates distinct differentiation processes in the peripheral and central immune systems. Given the essential function of RORγt in T_H17 cells, RORγt inhibitors have been developed for treatment of T_H17-dependent autoimmunity [10, 11, 12, 13, 14]. Such inhibitors are also expected to interfere with RORγt function in thymocytes and thus impair T cell development, which could eventually lead to the development of lymphoma [6]. Development of novel RORγt-based treatments that specifically target T_H17-mediated autoimmunity is as such of high order [6].

RORγt is a steroid nuclear receptor that consists of three domains [15, 16]: a conserved DNA-binding domain with two zinc finger motifs responsible for DNA-binding; a conserved ligand-binding domain with a C-terminal AF2 motif responsible for recruiting steroid receptor co-activator (SRC) to stimulate gene expression [17, 18]; and a hinge domain between the DNA- and ligand-binding domains. Upon ligand binding, RORγt recruits SRC and binds to target DNA to regulate target gene expression. To date, no function has been assigned to the RORγt hinge domain, which is generally believed to serve as a flexible linker region between the conserved and functionally important DNA-binding and ligand-binding domains. However, the observation that the hinge domain is not conserved between three members of the ROR family [19], suggests a potentially unique function.

By mutagenesis, we identified a mutant form of RORγt, which contains two amino acid mutations within the non-conserved hinge region of RORγt (called RORγt^M in this manuscript) that specifically disrupted RORγt function in T_H17 differentiation, but not thymocyte development. Mice expressing RORγt^M in the endogenous RORγt locus (called *RORγt*$^{M/M}$ mice here) lacked T_H17 differentiation, but had normal overall T cell development and developed most lymph nodes, including gut-associated mesenteric lymph nodes, but lacked Peyer's patches. RORγt^M interfered with ubiquitination of RORγt at lysine 69 (K69). Similar to RORγt^M, mutation of K69 to arginine (K69R) to prevent ubiquitination selectively impaired RORγt-mediated T_H17 differentiation but not thymocyte development. Our study thus distinguishes between RORγt function in T_H17 differentiation and thymocyte development, and reveals distinct mechanisms for these two RORγt-regulated processes.

Results

RORγt supports *in vitro* T cell development and T_H17 differentiation

To evaluate the function of RORγt function in T_H17 differentiation and thymocyte development, we investigated the structural requirements of the RORγt protein for these two

functions. In an *in vitro* differentiation system, sorted $CD4^{-}CD8^{-}$ (DN) thymocytes from wild-type and *RORγt*$^{-/-}$ mice were cultured on OP9-DL4 stromal cells to induce differentiation [20]. Wild-type, but not *RORγt*$^{-/-}$ DN thymocytes differentiated into $CD4^{+}CD8^{+}$ DP and $CD4^{+}$ (CD4SP) thymocytes (Fig. 1a). Both wild-type and *RORγt*$^{-/-}$ DN thymocytes were negative for RORγt expression, but DP thymocytes differentiated from wild-type DN thymocytes expressed RORγt (Fig. 1b). Consistent with previous observation, RORγt was up-regulated in DP thymocytes and was required for their survival [5, 7, 18]. A population of $TCR^{lo}CD24^{hi}CD8^{+}$ thymocytes developed from both wild-type and *RORγt*$^{-/-}$ DN thymocytes (Supplementary Fig. 1a) prior to the DP stage [21]. Thus, we used the percentage of $CD4^{+}$ cells, including both $CD4^{+}CD8^{+}$ DPs and mature $CD4^{+}$ SPs, to evaluate the efficiency of thymocyte development (Fig. 1a, **right panel**). To assess the role of RORγt in thymocyte development, we transduced *RORγt*$^{-/-}$ DN thymocytes with a retrovirus expressing RORγt-GFP or empty virus alone (EV-GFP) as control. Thymocyte development was rescued only in RORγt-GFP^{+} cells, but not in EV-GFP^{+} cells (Fig. 1c) or in GFP- cells that were not transduced by virus (Supplementary Fig. 1b). Furthermore, thymocyte development was not rescued by expression of RORγt mutants that cannot bind target DNA (RORγt-DBD) or the co-activator SRC (RORγt-AF2) (Fig. 1c), although both mutants were expressed at the equivalent levels as wild-type RORγt (Supplementary Fig. 1c), consistent with the notion that DNA-binding activity and AF2-mediated recruitment of co-activator SRC are required for RORγt to support thymocyte development [18].

To establish an *in vitro* T_H17 differentiation assay, splenic $CD4^{+}$ T cells isolated from wild-type or *RORγt*$^{-/-}$ mice were cultured in T_H17 priming conditions. *RORγt*$^{-/-}$ $CD4^{+}$ T cells, but not wild-type $CD4^{+}$ T cells, were defective in T_H17 differentiation (Fig. 1d), and lacked RORγt expression (Supplementary Fig. 1d). T_H17 differentiation of *RORγt*$^{-/-}$ T cells was rescued in retrovirally transduced RORγt-GFP^{+} cells, but not EV-GFP^{+} (Fig. 1e) or in GFP^{-} non-transduced cells (Supplementary Fig. 1e). Similar to RORγt-mediated T cell development, retroviral expression of RORγt-DBD and RORγt-AF2 at the same level as RORγt-GFP (Supplementary Fig. 1f) failed to rescue Th17 differentiation (Fig. 1e). Therefore, both T cell development and T_H17 differentiation depend on RORγt DNA-binding activity and AF2-mediated recruitment of co-activator SRC. Consistent with RORγt up-regulation of anti-apoptotic Bcl-x_L to enhance thymocyte survival [5, 7], retroviral expression of anti-apoptotic Bcl-x_L (Bcl-x_L-GFP) partially rescued differentiation of DP thymocytes from *RORγt*$^{-/-}$ thymocytes (Fig. 1f). However, Bcl-x_L-GFP could not rescue T_H17 differentiation in *RORγt*$^{-/-}$ T cells (Fig. 1g), indicating distinct mechanisms involved in RORγt-regulated T_H17 differentiation and thymocyte development.

Two amino acids are critical for T_H17 differentiation but not T cell development

As mutations affecting the RORγt DNA-binding activity and the AF2 motif of ligand-binding domain interfered with both thymocyte development and T_H17 differentiation, we extended the search for structural RORγt elements differentially required for these functions by introducing mutations in the RORγt hinge domain. By mutating consecutive stretches of five amino acids to alanines (alanine scanning), we created 33 mutants covering the hinge region (amino acids 76–240, Fig. 2a). *RORγt*$^{-/-}$ DN thymocytes or peripheral *RORγt*$^{-/-}$ $CD4^{+}$ T cells transduced with retroviruses expressing RORγt-GFP or alanine-mutant

RORγt were assessed for rescued thymocyte development and T_H17 differentiation *in vitro,* as described above. 20 out of 33 mutants such as 176–180A and 191–195A (supplementary Fig. 1g) rescued both thymocyte development and T_H17 differentiation. Seven mutants (**e.g. 76–80A in** Fig. 2b and 181–185A in supplementary Fig. 1g) markedly impaired both thymocyte development and T_H17 differentiation. These mutants were scattered across the entire hinge domain (Fig. 2c, top panel), indicating that functionally important motifs of RORγt for both functions are not clustered together.

Six mutants, including 91–95A (Fig. 2b) and 151–155A (Supplementary Fig. 1g) preferentially impaired T_H17 differentiation, with limited effect on thymocyte development, indicating a selective requirement of these two regions (amino acids 91–105 and 151–165) for T_H17 differentiation (Fig. 2c, top panel). 151–165 mutants maintained more than 50% activity during T_H17 differentiation, while mutant 91–95A maintained the majority of activity in thymocyte development, but could not support T_H17 differentiation (Fig. 2c, top panel). When expressed as the ratio of the percentage of rescued thymocyte development versus percentage of rescued T_H17 differentiation, mutant 91–95A showed the biggest difference between the ability to support thymocyte development and inability to support T_H17 differentiation (Fig. 2c, bottom panel).

We further defined which amino acids were critical for distinguishing between the two RORγt-regulated functions in mutant 91–95A. The amino acid sequence from 91–95 is DSLHA and our alanine scan did not change the last A. To investigate the requirement for the first four amino acids, we created two three-alanine mutants covering these four amino acids: 91–93A and 92–94A. Similar to mutant 91–95A, 91–93A and 92–94A supported thymocyte development (Fig. 2d, top panel), but neither supported T_H17 differentiation (Fig. 2d, bottom panel) when retrovirally expressed in *RORγt*$^{-/-}$ T cells. Additionally, a S92A-L93A mutant rescued thymocyte development (Fig. 2e, top panel) but not T_H17 differentiation (Fig. 2e, bottom panel) in *RORγt*$^{-/-}$ T cells. The single mutant S92A preserved both functions, whereas mutant L93A significantly impaired both thymocyte development and T_H17 differentiation (Fig. 2e). Immunoblotting confirmed that all mutants were expressed at equivalent levels with wild-type RORγt (Supplementary Fig. 1h). S92A-L93A was the minimum mutation sufficient to distinguishly regulate RORγt-dependent thymocyte development and T_H17 differentiation (Fig. 2f). We have thus identified a RORγt mutation (hereafter called RORγt^M) that specifically disrupts RORγt-mediated T_H17 differentiation, but not thymocyte development.

RORγt^M cannot induce genes critical for Th17 differentiation

Th17 differentiation depends on RORγt-regulated gene expression [22]. To assess the global effects of RORγt^M on T_H17 differentiation, we performed RNA sequencing (RNA-seq) and chromatin immunoprecipitation-DNA-seq (ChIP-seq) analyses of *RORγt*$^{-/-}$ T cells transduced with retrovirus expressing GFP only (EV-GFP), RORγt-GFP or RORγt^M-GFP (Fig. 3). The flag-tag fused to RORγt to immunoprecipitate RORγt-binding DNA fragments for ChIP did not affect RORγt expression or function in Th17 differentiation (Supplementary Fig. 2a,b). We found similar expression patterns between *RORγt*$^{-/-}$ T cells reconstituted with EV-GFP and RORγt^M-GFP, which was different for *RORγt*$^{-/-}$ T cells

reconstituted with RORγt-GFP (Fig. 3a), an observation confirmed by hierarchical clustering analysis (Fig. 3a). Many T_H17 signature genes, including *Il17a, Il17f, Il23r, Il1r, Ccr6, IL-17re and Il22* were down-regulated in EV-GFP$^+$*RORγt*$^{-/-}$ T cells compared to RORγt-GFP$^+$*RORγt*$^{-/-}$ T cells (Fig. 3b, left panel), confirming the defective Th17 differentiation. These T_H17 signature genes were also down-regulated in RORγt^M-GFP$^+$*RORγt*$^{-/-}$ T cells compared to RORγt-GFP$^+$*RORγt*-$^{-/-}$ T cells (Fig. 3b, right panel). ChIP-seq identified 21,917 RORγt-DNA binding peaks within gene loci such as *Il17* and *Il23r* (Fig. 3c) as well as *Il1r, Il17re, Rorc and Ccr6* (Supplementary Fig. 2c) known to be critical for T_H17 differentiation. Of 3,931 RORγt^M-DNA binding peaks identified in RORγt^M-GFP$^+$ cells, almost all (3886 out of 3931) overlapped with RORγt-DNA binding peaks. However, RORγt^M lost or showed significantly reduced DNA-binding peaks within important T_H17 gene loci (Fig. 3c and supplementary Fig. 2c), which correlated with their diminished expression (Fig. 3b). Greatly deduced binding to *Il17* and *Il23r* loci by RORγt^M compared to RORγt was confirmed by individual ChIP assays (Fig. 3d). Therefore, RORγt^M selectively loses DNA-binding sites and ability to activate genes required for T_H17 differentiation.

RORγt^M supports thymocyte development *in vivo*

To test the *in vivo* function of RORγt^M, we knocked-in exon 4, which contains the coding sequence for the two critical amino acids (S92-L93), in the *RORγt* locus (Supplementary Fig. 3a). A neomycin gene used for selection was also deleted by flp recombinase (Supplementary Fig. 3b) to avoid interfering with gene expression. *RORγt^M* expression was indicated by the detection of S92A-L93A mutations by sequence analysis of RORγt mRNA (Supplementary Fig. 3c). Mice expressing *RORγt^M* from the endogenous RORγt locus are called *RORγt*$^{M/M}$ hereafter. We first examined T cell development in *RORγt*$^{M/M}$ mice. Intracellular staining of RORγt showed equivalent expression of RORγt^M and RORγt in CD4$^+$CD8$^+$ DPs of corresponding mice (Supplementary Fig. 4a), suggesting appropriate RORγt^M expression during T cell development. *RORγt*$^{-/-}$ mice had dramatically reduced thymic cellularity (Fig. 4a) due to accelerated spontaneous apoptosis (Fig. 4b), while the thymic cellularity and survival of *RORγt*$^{M/M}$ thymocytes were almost equivalent to that of wild-type mice (Fig. 4a, b). Based on the surface CD44 and CD25 markers, DN thymocyte development in *RORγt*$^{-/-}$ or *RORγt*$^{M/M}$ mice was similar to wild-type (Supplementary Fig. 4b) [5]. The percentage (Fig. 4c) and absolute number (Supplementary Fig. 4c) of CD4$^+$ and CD4$^+$CD8$^+$ DP were reduced in *RORγt*$^{-/-}$ thymus compared to wild-type mice, while *RORγt*$^{M/M}$ mice had similar percentage and number of CD4$^+$ and CD4$^+$CD8$^+$ DP cells to those detected in wild-type mice. Moreover, while CD8$^+$ thymocytes in *RORγt*$^{-/-}$ mice were mostly immature TCR^{lo}CD24^{hi}, CD8$^+$ cells in *RORγt*$^{M/M}$ thymi were mostly TCR^{hi}CD24^{lo} mature cells, similar to wild-type mice (Fig. 4d). Compared to the enlarged cell size (FSC) (Fig. 4e) and markedly increased number of cells entering DNA synthesis (S) phase of the cell cycle, indicated by cells with >2N DNA (Fig. 4f) in *RORγt*$^{-/-}$ mice, *RORγt*$^{M/M}$ thymocytes had the same cell size and percentage of cells in S phase as the wild-type mice (Fig. 4e, f). In addition, RNA-seq indicated that the most prominent apoptotic molecule up-regulated in wild-type thymocytes compared to the *RORγt*$^{-/-}$ thymocytes was Bcl-x_L (encoded by *Bcl2l1*) (Fig. 4g). Many cell cycle regulators, including cyclins and cell division cycle proteins, displayed changes greater than 2-fold in *RORγt*$^{-/-}$ vs wild-type

thymocytes(Fig. 4g, top panel), consistent with the survival and cell cycle changes observed in *RORγt*$^{-/-}$ thymocytes. Changes in the expression of Bcl-x_L and cell cycle molecules were significantly less pronounced between *RORγt*$^{M/M}$ and wild-type thymocytes (Fig. 4g, bottom panel) than between *RORγt*$^{-/-}$ and wild-type thymocytes (Fig. 4g, top panel), suggesting that *RORγt*$^{M/M}$ thymocytes were phenotypically equivalent to wild-type, but not *RORγt*$^{-/-}$ thymocytes. As such, RORγt^{M} functions largely similarly to endogenous RORγt in supporting thymocyte development *in vivo*.

RORγt$^{M/M}$ mice have defective T_H17 differentiation

The distribution of naïve and memory T cells in *RORγt*$^{M/M}$ mice was similar to that observed in wild-type mice (Supplementary Fig. 5a,b). To determine the function of *RORγt*^{M} in T_H17 cells, we differentiated naïve spenic T cells from wild-type, *RORγt*$^{M/M}$ and *RORγt*$^{-/-}$ mice under Th1, T_H17, Th2 or Treg conditions. In contrast to wild-type T cells, and similar to *RORγt*$^{-/-}$ T cells, *RORγt*$^{M/M}$ T cells failed to differentiate into IL-17 producing cells (Fig. 5a, bottom panel), while there were no obvious differences in their ability to differentiate into T_H1 (Fig. 5a, top panel), T_H2 (Supplementary Fig. 5c) or Treg cells (Supplementary Fig. 5d) compared to wild-type cells, suggesting a selective defect in T_H17 differentiation. In *in vitro*-differentiated T_H17 cells, RORγt^{M} protein expression was equivalent to RORγt in wild-type cells (Fig. 5b), suggesting that defective T_H17 differentiation was not due to lack of RORγt^{M} expression. Development of EAE was attenuated in both *RORγt*$^{-/-}$ and *RORγt*$^{M/M}$ mice, compared to wild-type mice (Fig. 5c), with greatly reduced numbers of infiltrated CD45$^+$ lymphocytes, including Ly6G$^+$ neutrophils, CD3$^+$ T cells, CD19$^+$ B cells, and CD11b$^+$ monocytes recovered from the central nervous system (CNS) of *RORγt*$^{-/-}$ and *RORγt*$^{M/M}$ mice compared to wild-type mice (Fig. 5d, Supplementary Fig. 6a), indicating reduced inflammation. Analysis of infiltrated lymphocytes indicated reduced expression of *Il17a, Ifng* and *Csf2* mRNA in *RORγt*$^{M/M}$ and *RORγt*$^{-/-}$ mice compared to wild-type mice (Fig. 5e). Adoptive transfer of naïve CD4$^+$ T cells into *Rag1*$^{-/-}$ mice followed by induction of EAE also induced greatly attenuated EAE in *Rag1*$^{-/-}$ mice reconstituted with *RORγt*$^{-/-}$ or *RORγt*$^{M/M}$ CD4$^+$ T cells, in contrast to *Rag1*$^{-/-}$ mice reconstituted with wild-type CD4$^+$ T cells (Fig. 6a), with reduced numbers of infiltrated lymphocytes, including Ly6G$^+$ neutrophils, CD4$^+$ T cells and CD11b$^+$ monocytes (Fig.6b and supplementary Fig. 6b) and decreased *Il17a, Ifng* and *Csf2* mRNA expression in infiltrating cells (Fig. 6c,d). *Il17a* mRNA was the most reduced, consistent with the greatest reduction in the percentage (Fig. 6e) and absolute number (Fig. 6f) of IL-17$^+$IFNγ$^+$ and IL-17$^+$GM-CSF$^+$ T cells, which are believed to be pathogenic for EAE [3, 4, 23]. In contrast, the overall percentage of IFNγ$^+$ and GM-CSF$^+$ cells in *RORγt*$^{-/-}$ or *RORγt*$^{M/M}$ reconstituted *Rag1*$^{-/-}$ mice were not obviously changed compared to wild-type reconstituted *Rag1*$^{-/-}$ mice (Fig. 6e,f), demonstrating selective defects in the differentiation of T_H17 cells. A similar specific reduction of IL-17$^+$ cells, but not IFN-γ$^+$ cells was also observed in CD4$^+$ T cells from draining lymph nodes, and to a lesser extent in CD4$^+$ T cells from spleens (Supplementary Fig. 6c). We did not observe differences in the expression of *Foxp3* in T cells from EAE-induced wild-type and *RORγt*$^{M/M}$ mice (Supplementary Fig. 6d).

Next we assessed the ratio of representative pathogenic and nonpathogenic gene expression in wild-type and *RORγt*$^{M/M}$ CD4+ T cells differentiated with either TGF-β + IL-6 or pathogenic TGF-β + IL-6 + IL-23 T_H17 priming conditions. The expression of nonpathogenic genes did not generally change more than 2 fold between wild-type and *RORγt*$^{M/M}$ T cells in either priming conditions (Fig. 6g). However, many pathogenic genes showed higher expression in wild-type compared to *RORγt*$^{M/M}$ T cells under non-pathogenic priming conditions (Fig. 6g). Some pathogenic genes had lower expression in wild-type compared to *RORγt*$^{M/M}$ T cells, but usually less than 2 fold change (Fig. 6g). All the pathogenic genes detected were expressed higher in wild-type than in *RORγt*^{M} T cells in the presence of IL-23 (Fig. 6g). When analyzing pathogenic and nonpathogenic gene expression in T cells obtained from EAE-induced mice, many pathogenic genes showed higher expression in wild-type T cells, whereas some showed lower expression in wild-type, but usually less than 2 fold change compared to *RORγt*^{M} T cells (Fig. 6h). Therefore, *RORγt*$^{M/M}$ T cells showed lower pathogenic potential, a loss of function in supporting T_H17 differentiation and induction of EAE *in vivo*.

RORγt$^{M/M}$ mice develop lymph nodes, but not Peyer's patches

Because *RORγt*$^{-/-}$ mice typically lack all lymph nodes [5], we examined lymph nodes development in *RORγt*$^{M/M}$ mice. In contrast to *RORγt*$^{-/-}$ mice, *RORγt*$^{M/M}$ mice had almost all lymph nodes examined, including aorta lymph nodes and gut-associated mesenteric lymph nodes (Table 1 and Fig. 7a). While inguinal lymph nodes were developed but smaller than those found in wild-type mice, reflected by the reduced cellularity (Fig. 7a). Consistently, the number of ILC3, which are enriched for lymphoid tissue inducer (LTi) was comparable to wild-type in mesenteric lymph nodes of *RORγt*$^{M/M}$ mice (Supplementary Fig. 6e, f). However, *RORγt*$^{M/M}$ mice failed to develop Peyer's patches similar to *RORγt*$^{-/-}$ mice (Table 1 and Fig. 7a), consistent with the evidence indicating that development of Peyer's patches and other peripheral lymph nodes depend on different pathways [24, 25]. *RORγt*^{M} is thus able to support the development of most lymph nodes, except Peyer's patches.

RORγt^{M} interferes with the ubiquitination of RORγt at lysine 69

To understand how the two-alanine mutation in RORγt^{M} affects RORγt function, we first monitored RORγt^{M} activity using a RORγt-luciferase reporter. RORγt recruits the transcription co-activator SRC1 via an AF2 motif within the ligand-binding domain [18, 26]. RORγt^{M} interacted with SRC1 and stimulated RORγt reporter activity similarly to wild-type RORγt (Supplementary Fig. 7a,b). RORγt is ubiquitinated in T_H17 cells [26]. Comparison of the RORγt ubiquitination patterns in cells isolated from wild-type, *RORγt*$^{-/-}$ and *RORγt*$^{M/M}$ mice indicated that the ubiquitination of RORγt^{M} was reduced in differentiated T_H17 cells (Fig.8a, left panel) and thymocytes (Fig.8a, right panel). We then immunoprecipitated RORγt and RORγt^{M} for mass spectrometric analysis of ubiquitinated lysines (K). Digesting ubiquitinated K leaves a GG isopeptide linked to K, which can be easily detected using mass spectrometry as an increased mass of 114.102 Da [27]. We detected ubiquitination signals at lysine 69 (K69) in wild-type RORγt, but not RORγt^{M} immunoprecipitated from differentiated T_H17 cells (data not shown). We then monitored RORγt ubiquitination in HEK 293T cells transfected with wild-type RORγt or RORγt^{M} and

HA-tagged ubiquitin, followed by immunoprecipitation for RORγt. Ubiquitinated RORγt^{M} was reduced compared to wild-type RORγt (Fig. 8b). To specifically evaluate K69 ubiquitination, we generated a mutant RORγt in which all 23 lysines, except K69, were mutated to arginines (RORγt-K69), so that only K69 can be ubiquitinated. RORγt-K69 was polyubiquitinated at K69 in HEK 293T cells (Fig. 8b), while introduction of the L92A-S93A mutation to RORγt-K69 (RORγt^{M}-K69) markedly impaired K69 ubiquitination (Fig. 8b), confirming that two amino acid mutations in RORγt^{M} interfere with K69 ubiquitination. Mutant 91–95A, but not three alanine scanning mutants 151–155A, 156–160A and 161–165A greatly impaired RORγt ubiquitination at K69 (Supplementary Fig.7c). We next determined whether the polyubiquitin chains on RORγt-K69 were K63- or K48-linked [28]. Mutating all seven Ks within HA-ubiquitin to arginines [K(7)R] or mutating only K63 to arginine (K63R) prevented RORγt-K69 ubiquitination, whereas mutating all Ks within HA-ubiquitin except K63 to arginines (K63) did not affect RORγt-K69 ubiquitination (Fig. 8c). This suggests the formation of K63-linked polyubiquitin chains at RORγt K69 residue. In contrast, mutating K48 of HA-ubiquitin to arginine (K48R) did not affect RORγt-K69 ubiquitination, whereas mutating all Ks of HA-ubiquitin except K48 to arginines (K48) prevented RORγt-K69 ubiquitination (Fig. 8c), indicating that polyubiquitin chains at RORγt K69 were not K48-linked. An important function of ubiquitination is to regulate protein degradation [28], ubiquitination was reported to regulate RORγt stability [29, 30, 31, 32]. However, RORγt^{M} protein expression showed no difference compared to wild-type RORγt at various times after treatment of differentiated T_H17 cells with the protein synthesis inhibitor cycloheximide (CHX) (Supplementary Fig. 7d,e), indicating that the degradation rate of RORγt^{M} was same as wild-type RORγt and correlating with the observation that changes in RORγt^{M} ubiquitination were not due to K48-linked polyubiquitin chains that target proteins for degradation [28].

To determine the function of K69 ubiquitination in RORγt-regulated function, we mutated RORγt K69 to arginine (mutant K69R) to prevent ubiquitination. As a control, we mutated RORγt K81 to arginine (mutant K81R), as K81 was not ubiquitinated in mass spectrometric analysis. K69R interacted with SRC1 and stimulated RORγt reporter activity similar to RORγt^{M} and RORγt in HEK 293T cells (Supplementary Fig. 7b,f). In thymocyte development and T_H17 differentiation assays, retroviral expression of K69R rescued 90% of thymocyte development in *RORγt*$^{-/-}$ thymocytes, similar to wild-type RORγt and K81R, and slightly greater than thymocyte development supported by RORγt^{M} (Fig. 8d,e), suggesting that K69 ubiquitination is not essential for RORγt-mediated thymocyte development. In contrast, K69R rescued only about 45% of T_H17 differentiation in *RORγt*$^{-/-}$ T cells, which was markedly reduced compared to wild-type RORγt and K81R (Fig. 8d,e), and correlated with reduced expression of T_H17 signature genes, including *Il17a, IL17f*, and *Ccl20* (Fig. 8f), as well as binding to the IL-17 promoter (Fig. 8g) in K69R-transduced *RORγt*$^{-/-}$ T cells. Therefore, K69 ubiquitination, although dispensable for thymocyte development, is required to promote T_H17 differentiation. However, because K69R was more potent than RORγt^{M} in supporting T_H17 differentiation, lack of K69 ubiquitination is only partially responsible for failed Th17 differentiation observed in the *RORγt*$^{M/M}$ T cells.

Discussion

In this study, we identified a two amino acid mutation in the hinge region of RORγt that allows normal thymocyte development, but not T_H17 differentiation. While *RORγt*$^{-/-}$ mice exhibit multiple defects, including thymocyte and ILC3 development, lymph node genesis and T_H17 differentiation, *RORγt*$^{M/M}$ mice exhibited a specific defect in Th17 differentiation, while maintaining thymocyte development. *RORγt*$^{M/M}$ mice also developed ILC3 cells, but these ILC3 were defective in the production of IL-17 cytokine (data not shown). Therefore, *RORγt*^{M} preserves the function to instruct T and ILC3 development, but selectively disrupts the IL-17 production function of mature cells. We further demonstrated that the two amino acid mutation impaired ubiquitination of RORγt at K69 that is selectively required for T_H17 differentiation but not thymocyte development.

RORγt$^{-/-}$ mice have a high incidence of thymic lymphoma, likely due to dysregulated thymocyte development, including cell cycle and apoptosis changes [6]. Because thymocyte development in *RORγt*^{M} mice is largely normal, lymphoma development seems unlikely. Indeed, we did not detected lymphoma among more than 160 *RORγt*^{M} mice analyzed, including 25 mice 24 week old, 8 mice 37–39 week old and 7 mice older than 39 weeks (results not shown), while more than 50% of *RORγt*$^{-/-}$ mice die of lymphoma prior to 39 week of age [6]. These result support the idea that lymphoma in *RORγt*$^{-/-}$ mice results from abnormal thymocyte development.

The RORγt S92A-L93A mutations were the minimum alterations in the hinge region that selectively disrupted RORγt function in T_H17 differentiation without affecting thymocyte development. Although S92 is a potential phosphorylation site, mutant S92A, which cannot be phosphorylated, did not affect RORγt function. In contrast, mutant L93A affected both RORγt-mediated thymocyte development and T_H17 differentiation. Whereas, two amino acid mutation, S92A-L93A (RORγt^{M}), can maximally separate RORγt function in thymocytes and T_H17 differentiation. RORγt^{M} did not affect RORγt activity, recruitment of the co-activator SRC1 and stimulation of a RORγt reporter, suggesting that two amino acid mutation does not affect overall RORγt function. However, RORγt^{M} impairs the ubiquitination of K69 that is required for T_H17 differentiation, but not thymocyte development. Therefore, post-translational ubiquitination plays an important role in distinguishing RORγt function in T_H17 differentiation versus thymocyte development. Although ubiquitination is known to regulate protein degradation [28], K69R and RORγt^{M} do not affect RORγt protein levels, and thus does not support the function of K69 ubiquitination in the regulation of RORγt stability. This is further confirmed by K63- but not K48-linked ubiqutination at K69 of RORγt. The fact that K69 locates in the DNA-binding domain and K69R impairs RORγt-binding to the IL-17 locus supports that RORγt^{M} affects DNA-binding activity selectively in T_H17 cells via interfering with K69 ubiquitination. This possibility is strengthened by our global analysis indicated that RORγt^{M} failed to bind and stimulate genes critical for T_H17 differentiation, whereas it did not significantly affect the expression of cell survival and cell cycle genes critical for thymocyte development. It still remains to be determined how K69 ubiquitination is selectively required for T_H17 differentiation but not thymocyte development. One of the possibilities is that K69 ubiquitination induces the recruitment of a co-factor to RORγt specifically in Th17 cells,

which can be determined by comparing RORγt-associated proteins between Th17 cells and thymocytes. In addition, the enzymes responsible for modifying K69 of RORγt remain unknown. Identification of these enzymes will facilitate the development of drugs that specifically target RORγt-mediated pathological autoimmune T_H17 responses, without interfering with thymocyte development or lymph node genesis.

RORγt mutations reported in humans result in susceptibility to fungal and mycobacteria infection [33]. However, these RORγt mutations locate in either the DNA-binding domain or the ligand-binding domain. Humans bearing RORγt mutations also have defects in lymph node genesis and thymocyte apoptosis [33], consistent with the phenotypes observed in *RORγt*$^{-/-}$ mice, and suggesting function conservation between human and mouse RORγt. It will be important to investigate if modifications of the S92-L93 motif identified in mice also distinguishes the thymocyte development and Th17 differentiation function of RORγt in humans.

Materials & Methods

Mice

The *RORγt*$^{-/-}$ (*Rorc2*$^{-/-}$) mouse strain was described previously [5]. Both the targeting vector and the knock-in *RORγt*$^{M/M}$ mice were designed and generated by Biocytogen LLC. Rosa-Flp (008600) and *Rag1*$^{-/-}$ (002216) mice were purchased from the Jackson Laboratory. For all experiments, mice were 6–12 weeks of age; age-matched littermates were used in experimental groups, and all groups contained five mice unless stated otherwise. Mice were bred and housed under specific pathogen-free (SPF) conditions in the Animal Resource Center at the Beckman Research Institute of City of Hope under protocols approved by the Institutional Animal Care and Use Committee.

Plasmids and Retrovirus

The retroviral vector MIGR (murine stem cell virus [MSCV]-IRES-GFP) was a gift from Dr. Warren S. Pear (University of Pennsylvania, Philadelphia, PA) and used to clone *RORγt* or *BCL-xL* cDNA as described previously. Mutant *RORγt* vectors were prepared using a site-directed mutagenesis kit from Agilent Technologies. pRK5-HA-ubiquitin constructs (a gift from Ted Dawson, Addgene #17603 -17608) for expressing HA-tagged wild-type and mutant ubiquitin were obtained from Addgene. Retroviruses were packaged in a Platinum-Eco cell line from Cell Biolabs as described previously [26]. Briefly, retroviral expression plasmids were transfected into Platinum-Eco packaging cells using Lipofectamine 2000 (thermofisher scientific). Viral supernatants were collected 72 h later, passed through 0.4-μm filters, and stored at −80°C until use.

Flow cytometry and cell sorting

Tissues were homogenized by crushing with the head of a 1-ml syringe in a petri dish, followed by straining through a 40-μm nylon filter. Red Blood Cell Lysing buffer (Sigma-Aldrich) was used for red cell lysis and remaining cells were counted. Antibodies used for flow cytometry staining are listed in Supplementary Table 1. For intracellular cytokine staining, cells obtained from *in vitro* cultures were incubated for 4–5 h with 50 ng/ml PMA,

750 ng/ml ionomycin (both from Sigma-Aldrich), and 10 μg/ml brefeldin A (BD Biosciences) in a tissue culture incubator at 37°C. Cells were resuspended in Fixation/Permeabilization solution and intracellular cytokine staining was performed (BD Cytofix/Cytoperm Kit; BD Biosciences). For sorting double-negative thymocytes, thymocytes from C57BL/6 or *RORγt*$^{-/-}$ mice were stained with 7-AAD and antibodies against Thy1.2, CD4 and CD8 (listed in Life Sciences Reporting System item 9). Specific Thy1.2^{+}/CD4^{-}/CD8^{-} populations were sorted using a FACSAria (BD Biosciences).

T cell development assay

Electronically sorted double-negative thymocytes (Thy1.2^{+}/CD4^{-}/CD8^{-}) were cultured at 5×10^{5}/ml overnight on an 80% confluent OP9-DL4 monolayer (generous gift from Dr. Ellen Rothenberg, Caltech) in flat-bottom 24-well culture plates with αMEM (MEM α medium; Invitrogen Life Technologies) supplemented with 20% FBS, 100 U/ml penicillin-streptomycin, 2 mM L-glutamine (Invitrogen Life Technologies), and 5 ng/ml recombinant murine IL-7 (PeproTech). The following day, co-cultures were transduced by spin infection (1200 g, 30°C for 2 h) using retroviral supernatants in the presence of 8 mg/ml polybrene (Sigma-Aldrich). After spin infection, viral supernatant was replaced with culture media containing 5 ng/ml recombinant murine IL-7. 72 h post-transduction, co-cultures were harvested for flow cytometry analysis.

CD4^{+} T cell isolation and *in vitro* T$_H$17 differentiation assay

Naive CD4^{+} T cells were purified from C57BL/6, *RORγt*$^{-/-}$, or *RORγt*$^{M/M}$ mice by negative selection using CD4^{+} T Cell Isolation Kit II (Miltenyi Biotec). Suspensions of 4×10^{5} cells/ml Iscove's modified DMEM (Cellgro) containing 2 mM L-glutamine, 50 mM 2-ME, 100 U/ml penicillin, 100 mg/ml streptomycin, and 10% FBS were cultured in 24-well plates pre-coated with 0.2 mg/ml goat anti-hamster antibody (MP biomedicals) for three days. The medium was supplemented with 0.25 μg/ml hamster anti-CD3 (145-2C11; eBioscience), 1 μg/ml hamster anti-CD28 (37.51; eBioscience), and polarizing cytokines: 2 ng/ml TGF-β (Peprotech), 20 ng/ml IL-6 (Peprotech), 5 μg/ml anti-IL-4 (11B11), and 5 μg/ml anti-IFNγ (XMG 1.2) for T$_H$17 differentiation; 20 ng/ml IL-23 (Miltenyi Biotec) was also added when inducing pathogenic T$_H$17 cells. 20 ng/ml IL-12 (Peprotech) and 5 μg/ml anti-IL-4 for T$_H$1 differentiation; 10 ng/ml IL-4 and 10 μg/ml anti-IFNγ for T$_H$2 differentiation; or 5 ng/ml TGF-β for Treg differentiation. For retroviral transduction, T cells were first activated with 0.25 μg/ml hamster anti-CD3 (145-2C11; eBioscience), 1 μg/ml hamster anti-CD28 (37.51; eBioscience) in 24-well plates pre-coated with 0.2mg/ml goat anti-hamster antibody for 24 h, then spin-infected with viral supernatants (1200 g, 30°C for 2 h) in the presence of 8 mg/ml polybrene (Sigma-Aldrich). After spin infection, viral supernatant was replaced by culture media with polarizing cytokines for in vitro differentiation.

RNA sequencing (RNA-seq) and analysis

To measure gene expression in the thymus of C57BL/6, *RORγt*$^{-/-}$ or *RORγt*$^{M/M}$ mice, two separate samples were collected on different days, and thymocytes from four (two male and two female) were pooled each day. For demonstrating the gene expression profile regulated by wild-type *RORγt* or *RORγt*$^{M/M}$ in *in vitro*-differentiated Th17 cells, CD4^{+} T cells were

enriched from *RORγt*$^{-/-}$ mice, transduced with retrovirus containing empty vector, wild-type *RORγt* or *RORγt*$^{M/M}$, then polarized under Th17 conditions for three days. Cells were processed for RNA isolation (Qiagen). Quality verification, library preparation, and sequencing were performed at City of Hope Integrative Genomics Core facility. Samples were sequenced on an IlluminaHiSeq 2000 using 75-bp paired end reads. Reads were aligned to the mm9 mouse genome using TopHat version 2.1.0 and Bowtie version 1.1.1. Differential expression was computed with Cufflinks version 2.2.1. Differentially expressed genes were filtered by significance at FDR-adjusted $P < 0.05$, and the ratio of fragments per kilobase of transcript per million mapped reads (FPKM) were at least two-fold changes between two of the populations. Clustering and heatmapping were performed using hierarchical clustering in R with pheatmap package version 1.0.8. For heat maps, expression values were scaled per gene.

Chromatin immunoprecipitation and DNA sequencing (ChIP-seq)

2×10^7 cells were incubated with 1% formaldehyde, to cross-link proteins with chromatin, for 5 min at room temperature. 125 mM glycine was added to stop the cross-linking reaction. To shear genomic DNA into 200–500 bp fragments, cell lysates were sonicated using a water-bath sonicator (Covaris S200). Cell lysates were centrifuged (12000 g, 10 min) and incubated with FLAG antibody (M2, Sigma-aldrich, listed in Life Sciences Reporting System item 9) or IgG controls, and magnetic protein A/G beads (Millipore). After extensive washing, DNA was eluted followed by reversion of the protein–DNA cross-linking. DNA was recovered for DNA-seq or qRT-PCR to quantify specific DNA fragments that were precipitated. Primers used in qRT-PCR were listed in Supplementary Table 1. Samples were sequenced on an IlluminaHiSeq 2000 using 75-bp paired end reads. Reads were aligned to the mm9 mouse genome using Bowtie version 1.1.1. Differential peaks were computed with MACS version 1.4.2 and bedtools version 2.17.0. Neighboring genes in the mm9 mouse genome were searched using webtools Cistrome Analysis Pipeline (at website: Cistrome.org/ap).

Quantitative real-time PCR (qRT-PCR)

qRT-PCR was performed using SsoFast EvaGreen Supermix (Bio-Rad) in a CFX96 Real-Time PCR Detection System (Bio-Rad), using primers as noted (Supplementary Table 1). The amplification efficiency of all primers has been tested, and the optimized conditions were used in all qRT-PCR reactions. Expression was calculated with the ΔΔxp method normalized to *β-actin*, and all measurements were performed in triplicate.

Apoptosis assays

Thymocytes were freshly isolated from wild-type, *RORγt*$^{-/-}$, or *RORγt*$^{M/M}$ mice and cultured in RPMI 1640 medium supplemented with 10% FBS, 100 U/ml penicillin-streptomycin, 2 mM L-glutamine at 1×10^6 cells/ml. Thymocytes were incubated at 37°C with 5% CO_2. Dead cells were detected by Annexin V-PE and 7-AAD staining (BD Bioscience), as described previously [34].

Induction and assessment of Experimental Autoimmune Encephalomyelitis (EAE)

Active EAE was induced and assessed as previously described [35]. Briefly, mice were immunized subcutaneously in the abdominal flank with 200 mg MOG_{35-55} and 400 mg Mycobacterium tuberculosis H37RA (Difco) in a 400 μl emulsion of equal volumes of water and complete Freund's adjuvant (Difco). Each mouse also received 0.4 mg purified Bordetella pertussis toxin in 200 μl PBS intraperitoneally on days 0 and 1. For reconstitution of T cells in *Rag1*$^{-/-}$ mice, 5×10^6 flow cytometry-sorted *CD4*$^+$ T cells from C57BL/6, *RORγt*$^{-/-}$, or *RORγt*$^{M/M}$ mice were intraperitoneally transferred into Rag1$^{-/-}$ mice, followed by active induction of EAE.

Western blot and immunoprecipitation

Cells were lysed in lysis buffer (0.5% Triton X-100, 20 mM HEPES, pH 7.4, 150 mM NaCl, 12.5 mM β-glycerophosphate, 1.5 mM $MgCl_2$, 10 mM NaF, 2 mM dithiothreitol, 1 mM sodium orthovanadate, 2 mM EGTA, 20 mM aprotinin, 1 mM phenylmethylsulfonyl fluoride). Protein from cell extracts (15 mg) was resolved using SDS-PAGE (10% gel), transferred to PVDF Membrane (Millipore), and Western blot was performed using relevant antibodies. Immunoprecipitation experiments were performed as described previously. In brief, cell extracts were incubated overnight with relevant antibodies and protein A/G beads at 4°C. After incubation, beads were washed four times with lysis buffer, resolved using SDS-PAGE, and analyzed using Western blot. Western blot primary antibodies were listed in Life Sciences Reporting System item 9.

Enrichment of ubiquitinated proteins by Agarose-TUBE1

A total of 1.5×10^8 thymocytes from C57BL/6, *RORγt*$^{-/-}$, or *RORγt*$^{M/M}$ mice, or 1.5×10^8 Th17 cells differentiated *in vitro* as described above, were lysed in 500 μl cell lysis buffer (50 mM Tris-HCl [pH 7.4], 150 mM NaCl, 1 mM EDTA, 1% NP-40, 10% glycerol, 1 mM PMSF). Cell lysates were incubated with 20 μl equilibrated Agarose-coupled Tandem Ubiquitin Binding Entity 1 (Agarose-TUBE1) (LifeSensors) at 4°C for 4 h. Agarose-TUBE1 was washed with 1 ml TBS-T (20 mM Tris-HCl [pH 8], 150 mM NaCl, 0.1% Tween-20) and suspended in SDS reducing sample buffer. Eluted samples were analyzed by Western blotting.

Statistical analysis

Prism software (Graphpad) was used for all statistical analyses. Unpaired Student's t tests and one-way analysis of variance (ANOVA) were used to compare experimental groups. A *P* value of less than 0.05 was considered statistically significant.

Supplementary Material

Refer to Web version on PubMed Central for supplementary material.

Acknowledgments

We thank J. C. Zuniga-Pflucker for providing DP9-DL4 stroma cell line, and Biocytogen for assisting with design and generation of the *RORγt*^{M} mice. This work was supported by grants from NIH R01-AI053147, NIH R01-AI109644 and institutional pilot funding. In addition, research reported in this publication was also supported by

the National Cancer Institute of the National Institutes of Health under award number P30CA33572, which includes work performed in the Animal Resource Center, Integrative Genomics, Analytical Cytometry, and Mass Spectrometry and Proteomics Cores supported by this grant. Dr. Zhaofeng Huang is supported by Science and Technology Department of Guangdong Province (2016A050503023). The content is solely the responsibility of the authors and does not necessarily represent the official views of the National Institutes of Health.

References

1. Ivanov, et al. The orphan nuclear receptor RORgammat directs the differentiation program of proinflammatory IL-17+ T helper cells. Cell. 2006; 126:1121–1133. [PubMed: 16990136]
2. Gaffen SL, Jain R, Garg AV, Cua DJ. The IL-23-IL-17 immune axis: from mechanisms to therapeutic testing. Nature reviews. Immunology. 2014; 14:585–600.
3. Codarri L, et al. RORgammat drives production of the cytokine GM-CSF in helper T cells, which is essential for the effector phase of autoimmune neuroinflammation. Nat Immunol. 2011; 12:560–567. [PubMed: 21516112]
4. El-Behi M, et al. The encephalitogenicity of T(H)17 cells is dependent on IL-1- and IL-23-induced production of the cytokine GM-CSF. Nat Immunol. 2011; 12:568–575. [PubMed: 21516111]
5. Sun Z, et al. Requirement for RORgamma in thymocyte survival and lymphoid organ development. Science. 2000; 288:2369–2373. [PubMed: 10875923]
6. Ueda E, et al. High incidence of T-cell lymphomas in mice deficient in the retinoid-related orphan receptor RORgamma. Cancer research. 2002; 62:901–909. [PubMed: 11830550]
7. Kurebayashi S, et al. Retinoid-related orphan receptor gamma (RORgamma) is essential for lymphoid organogenesis and controls apoptosis during thymopoiesis. Proceedings of the National Academy of Sciences of the United States of America. 2000; 97:10132–10137. [PubMed: 10963675]
8. Chen Y, et al. Anti-IL-23 therapy inhibits multiple inflammatory pathways and ameliorates autoimmune encephalomyelitis. The Journal of clinical investigation. 2006; 116:1317–1326. [PubMed: 16670771]
9. Eberl G, et al. An essential function for the nuclear receptor RORgamma(t) in the generation of fetal lymphoid tissue inducer cells. Nat Immunol. 2004; 5:64–73. [PubMed: 14691482]
10. Huh JR, Littman DR. Small molecule inhibitors of RORgammat: targeting Th17 cells and other applications. Eur J Immunol. 2012; 42:2232–2237. [PubMed: 22949321]
11. Burchill MA, Yang J, Vogtenhuber C, Blazar BR, Farrar MA. IL-2 receptor beta-dependent STAT5 activation is required for the development of Foxp3+ regulatory T cells. J Immunol. 2007; 178:280–290. [PubMed: 17182565]
12. Dang EV, et al. Control of T(H)17/T(reg) balance by hypoxia-inducible factor 1. Cell. 2011; 146:772–784. [PubMed: 21871655]
13. Sheridan C. Footrace to clinic heats up for T-cell nuclear receptor inhibitors. Nature biotechnology. 2013; 31:370.
14. Huang Z, Xie H, Wang R, Sun Z. Retinoid-related orphan receptor gamma t is a potential therapeutic target for controlling inflammatory autoimmunity. Expert opinion on therapeutic targets. 2007; 11:737–743. [PubMed: 17504012]
15. Sherlock JP, et al. IL-23 induces spondyloarthropathy by acting on ROR-gammat+ CD3+CD4−CD8− entheseal resident T cells. Nature medicine. 2012; 18:1069–1076.
16. Langrish CL, et al. IL-23 drives a pathogenic T cell population that induces autoimmune inflammation. J Exp Med. 2005; 201:233–240. [PubMed: 15657292]
17. Xie H, Huang Z, Wang R, Sun Z. Regulation of thymocyte survival by transcriptional coactivators. Critical reviews in immunology. 2006; 26:475–486. [PubMed: 17341189]
18. Xie H, Sadim MS, Sun Z. RORgammat recruits steroid receptor coactivators to ensure thymocyte survival. J Immunol. 2005; 175:3800–3809. [PubMed: 16148126]
19. Jetten AM, Kurebayashi S, Ueda E. The ROR nuclear orphan receptor subfamily: critical regulators of multiple biological processes. Progress in nucleic acid research and molecular biology. 2001; 69:205–247. [PubMed: 11550795]

20. Holmes R, Zuniga-Pflucker JC. The OP9-DL1 system: generation of T-lymphocytes from embryonic or hematopoietic stem cells in vitro. Cold Spring Harbor protocols. 2009; 2009 pdb prot5156.
21. Yui MA, Rothenberg EV. Developmental gene networks: a triathlon on the course to T cell identity. Nature reviews Immunology. 2014; 14:529–545.
22. Staschke KA, et al. IRAK4 kinase activity is required for Th17 differentiation and Th17-mediated disease. J Immunol. 2009; 183:568–577. [PubMed: 19542468]
23. Lee Y, et al. Induction and molecular signature of pathogenic TH17 cells. Nat Immunol. 2012; 13:991–999. [PubMed: 22961052]
24. Debard N, Sierro F, Kraehenbuhl JP. Development of Peyer's patches, follicle-associated epithelium and M cell: lessons from immunodeficient and knockout mice. Seminars in immunology. 1999; 11:183–191. [PubMed: 10381864]
25. van de Pavert SA, Mebius RE. New insights into the development of lymphoid tissues. Nature reviews Immunology. 2010; 10:664–674.
26. He Z, et al. Ubiquitination of RORgammat at Lysine 446 Limits Th17 Differentiation by Controlling Coactivator Recruitment. J Immunol. 2016; 197:1148–1158. [PubMed: 27430721]
27. Miller MJ, Barrett-Wilt GA, Hua Z, Vierstra RD. Proteomic analyses identify a diverse array of nuclear processes affected by small ubiquitin-like modifier conjugation in Arabidopsis. Proceedings of the National Academy of Sciences of the United States of America. 2010; 107:16512–16517. [PubMed: 20813957]
28. Jain R, et al. Interleukin-23-Induced Transcription Factor Blimp-1 Promotes Pathogenicity of T Helper 17 Cells. Immunity. 2016; 44:131–142. [PubMed: 26750311]
29. Lazarevic V, et al. T-bet represses T(H)17 differentiation by preventing Runx1-mediated activation of the gene encoding RORgammat. Nat Immunol. 2011; 12:96–104. [PubMed: 21151104]
30. Han L, et al. The E3 deubiquitinase USP17 is a positive regulator of retinoic acid-related orphan nuclear receptor gammat (RORgammat) in Th17 cells. J Biol Chem. 2014; 289:25546–25555. [PubMed: 25070893]
31. Wang X, et al. TRAF5-mediated Lys-63-linked Polyubiquitination Plays an Essential Role in Positive Regulation of RORgammat in Promoting IL-17A Expression. J Biol Chem. 2015; 290:29086–29094. [PubMed: 26453305]
32. Yang J, et al. Cutting edge: Ubiquitin-specific protease 4 promotes Th17 cell function under inflammation by deubiquitinating and stabilizing RORgammat. J Immunol. 2015; 194:4094–4097. [PubMed: 25821221]
33. Okada S, et al. IMMUNODEFICIENCIES. Impairment of immunity to Candida and Mycobacterium in humans with bi-allelic RORC mutations. Science. 2015; 349:606–613. [PubMed: 26160376]
34. Xie H, Huang Z, Sadim MS, Sun Z. Stabilized beta-catenin extends thymocyte survival by up-regulating Bcl-xL. J Immunol. 2005; 175:7981–7988. [PubMed: 16339534]
35. Ma J, Wang R, Fang X, Ding Y, Sun Z. Critical role of TCF-1 in repression of the IL-17 gene. PLoS One. 2011; 6:e24768. [PubMed: 21935461]

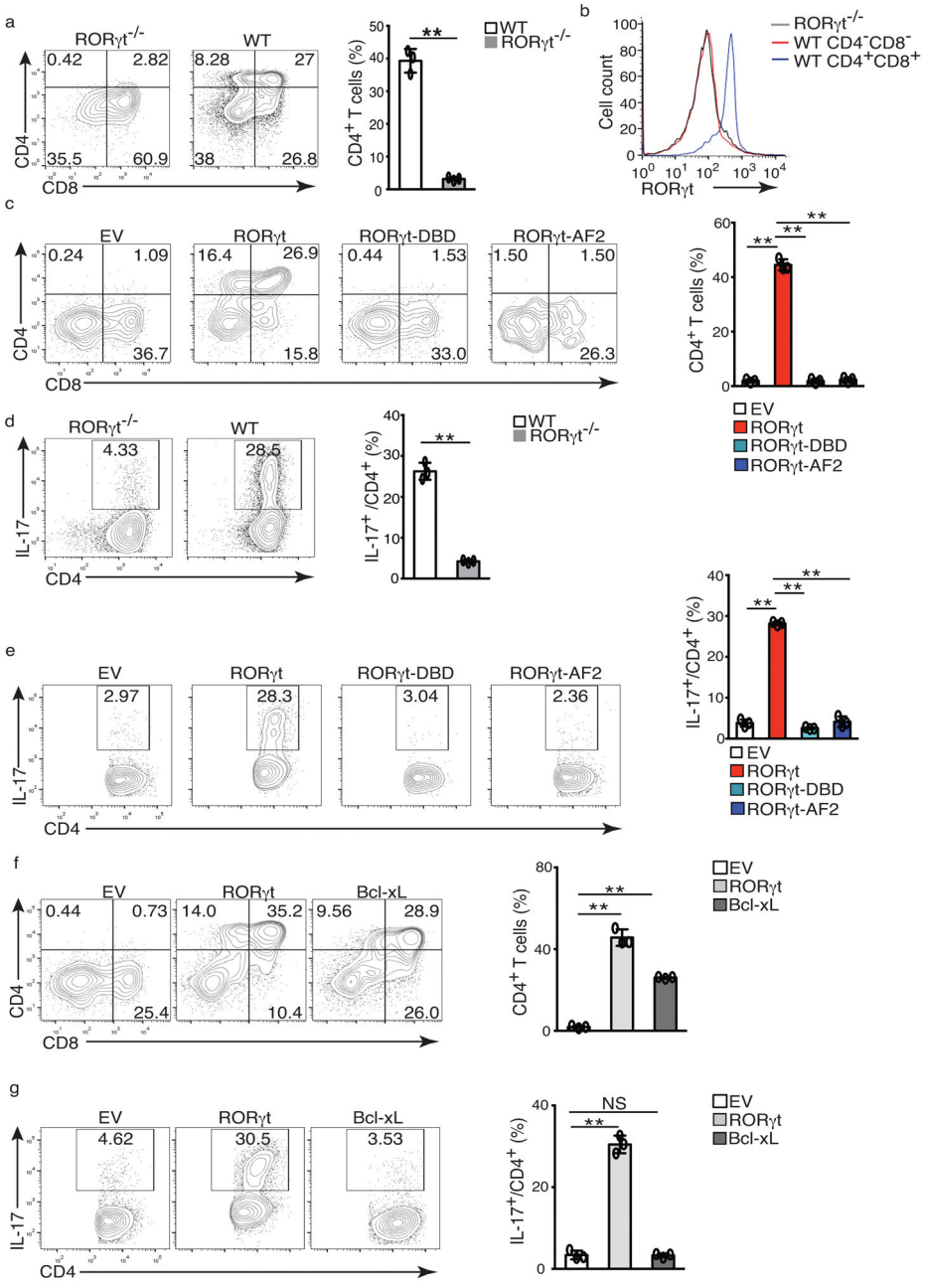

Figure 1. RORγt supports *in vitro* T cell development and T_H17 differentiation

(**a**) Flow cytometer analysis of CD4 and CD8 in *ex vivo* development of $CD4^-CD8^-$ thymocytes from wild type or *RORγt*$^{-/-}$ mice for three days. Right panel is the frequency of total $CD4^+$ thymocytes. (**b**) Flow cytometer analysis for RORγt expression by cells shown in **a**. (**c**) Flow cytometer analysis of *ex vivo* development of $CD4^-CD8^-$*RORγt*$^{-/-}$ thymocytes transduced with retrovirus expressing GFP only (EV), or together with RORγt or mutants incapable of binding DNA (RORγt-DBD) or co-activator (RORγt-AF2). Right panel is the percentage of $CD4^+$ among 7-AAD^- $Thy1.2^+GFP^+$ cells. (**d**) Flow cytometer analysis for IL-$17A^+$ cells in naïve WT or *RORγt*$^{-/-}$ $CD4^+$ T cells polarized under Th17

priming conditions for three days. Right panel is the percentage of IL-17A$^+$ cells among CD4$^+$ cells. (**e**) Flow cytometer analysis of IL-17A$^+$ cells in *RORγt*$^{-/-}$ CD4$^+$ T cells transduced with indicated retrovirus. Right panel is the percentage of IL-17A$^+$ cells among CD4$^+$GFP$^+$ cells. (**f**) Flow cytometer analysis of *ex vivo* development of CD4$^-$CD8$^-$ *RORγt*$^{-/-}$ thymocytes transdced with indicated retrovirus. Right panel is the quantification of the results. (**g**) Flow cytometer analysis of IL-17A$^+$ cells in *RORγt*$^{-/-}$ CD4$^+$ T cells transduced with indicated retrovirus. Right panel is the quantification of results. Data in right panel of **a**,**c**,**d**,**e,f,g** are mean ± s.e.m. $^{**}P < 0.01$, $^{***}P < 0.001$ (ANOVA test). Each symbol represents an individual experiment. Data are pooled from three experiments (**right panel of a**,**c**,**d**,**e,f,g**), or are from one experiment representative of three experiments (**b** and left panel of **a**,**c**,**d**,**e,f,g**),

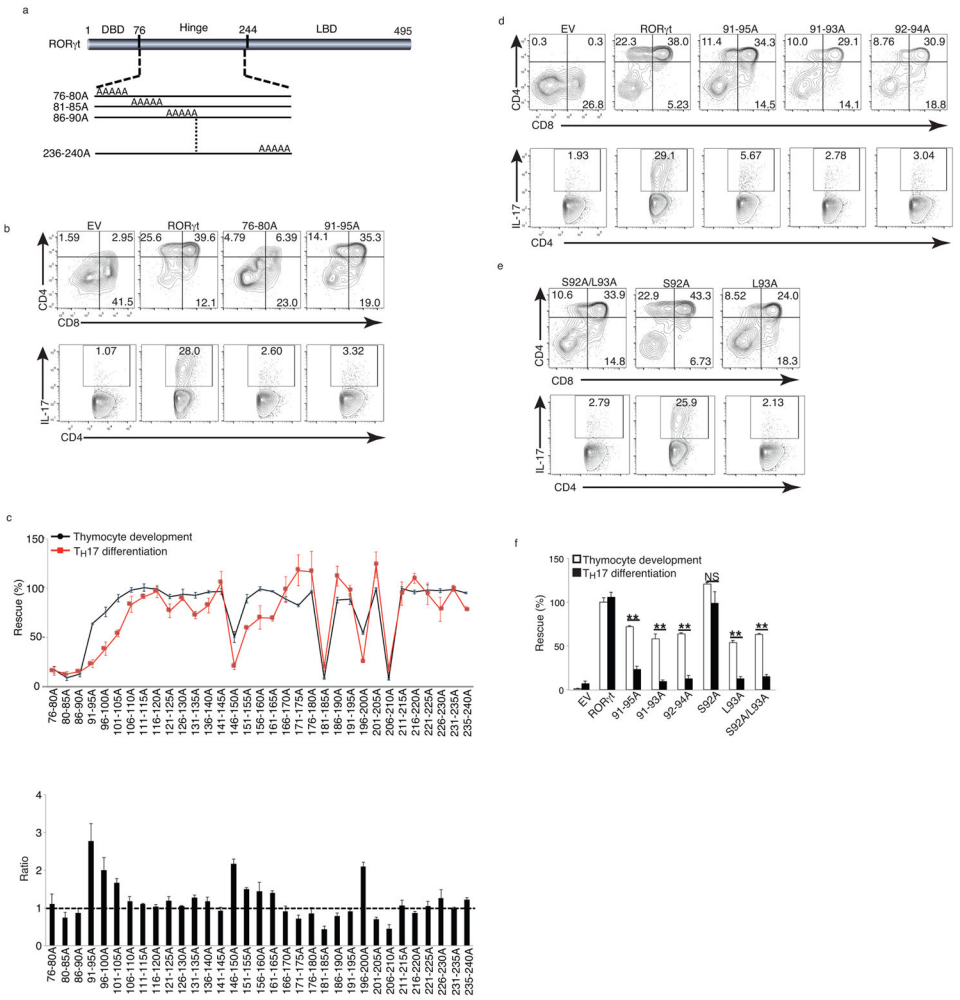

Figure 2. S92 and L93 are critical for T_H17 differentiation but not T cell development

(**a**) Schematic representation of RORγt structure and alanine-scanning mutants. Numbers indicate the positions of amino acids. DBD: DNA-binding domain. LBD: Ligand-binding domain. (**b**) Flow cytometer analysis of *ex vivo* thymocyte development (top panel) and T_H17 differentiation of *RORγt*$^{-/-}$ cells retrovirally expressing indicated RORγt. (**c**) Top panel is the percentage of rescued thymocyte development (black/circles) and T_H17 differentiation (red/squares) by indicated RORγt mutants relative to WT RORγt (defined as 100%). Bottom panel is the ratio of percentage of rescued thymocyte development to that of rescued Th17 differentiation. (**d and e**) Flow cytometer analysis of *ex vivo* thymocyte development (top panel) and T_H17 differentiation of *RORγt*$^{-/-}$ cells retrovirally expressing indicated RORγt (**f**) Quantification of the results shown in **d** and **e**. Data in **c**,**f** are mean ± s.e.m. $^{**}P < 0.01$, $^{***}P < 0.001$ (ANOVA test). Data are pooled from three experiments (**c**,**f**), or are from one experiment representative of three experiments (**b,d,e**),

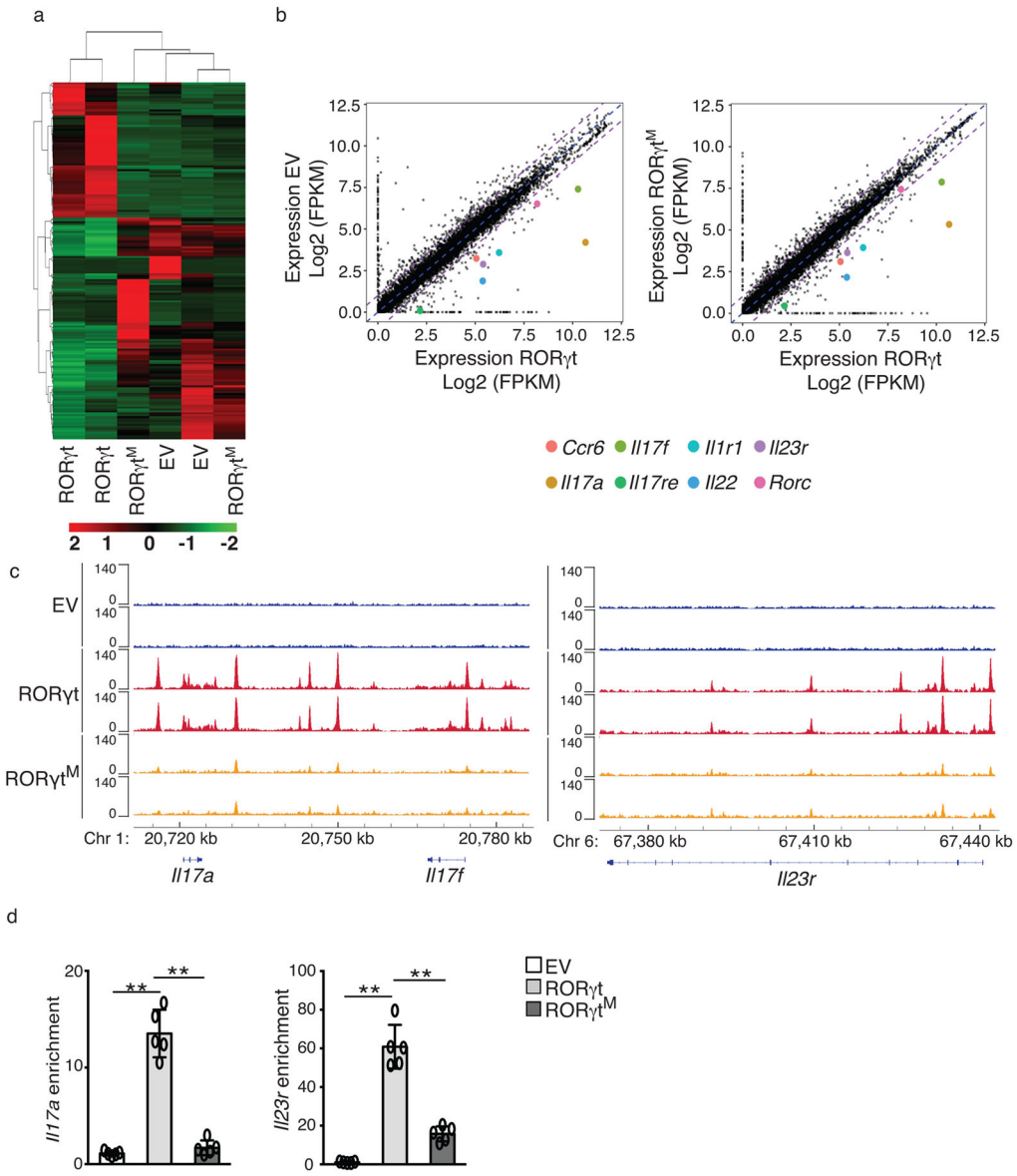

Figure 3. RORγt^{M} cannot induce genes critical for T_H17 differentiation

(**a**) Heatmap visualization of the up-regulated (red) and down-regulated (green) genes determined by RNA-seq assay in *RORγt*$^{-/-}$ CD4^{+} T cells retrovirally reconstituted with EV, WT RORγt, or RORγt^{M} and polarized under T_H17 conditions for three days. (**b**) Comparison of gene expression profiles between *RORγt*$^{-/-}$ CD4^{+} T cells reconstituted with EV and *RORγt* (left panel), and between *RORγt*$^{-/-}$ CD4^{+} T cells reconstituted with RORγt^{M} and RORγt (right panel). Colored dots represent selected critical T_H17 genes as indicated. Average fragments per kilobase of transcript per million mapped reads (FRKM) values of three replicates are shown. (**c**) ChIP assay identified RORγt DNA-binding peaks in *Il17a, Il17f*, and *Il23r* loci. (**d**) ChIP analysis of RORγt interaction with *Il17a* (left) and *Il23r* (right) loci in *RORγt*$^{-/-}$ CD4^{+} T cells retrovirally expressing EV, WT RORγt, or RORγt^{M}. Data are pooled from three experiments (**a**,**b**), or are from one experiment representative of

three experiments (**c**,**d**). Data in **d** are shown as mean ± s.e.m.; Each symbol represents an individual experiment. ** $p<0.01$ by ANOVA.

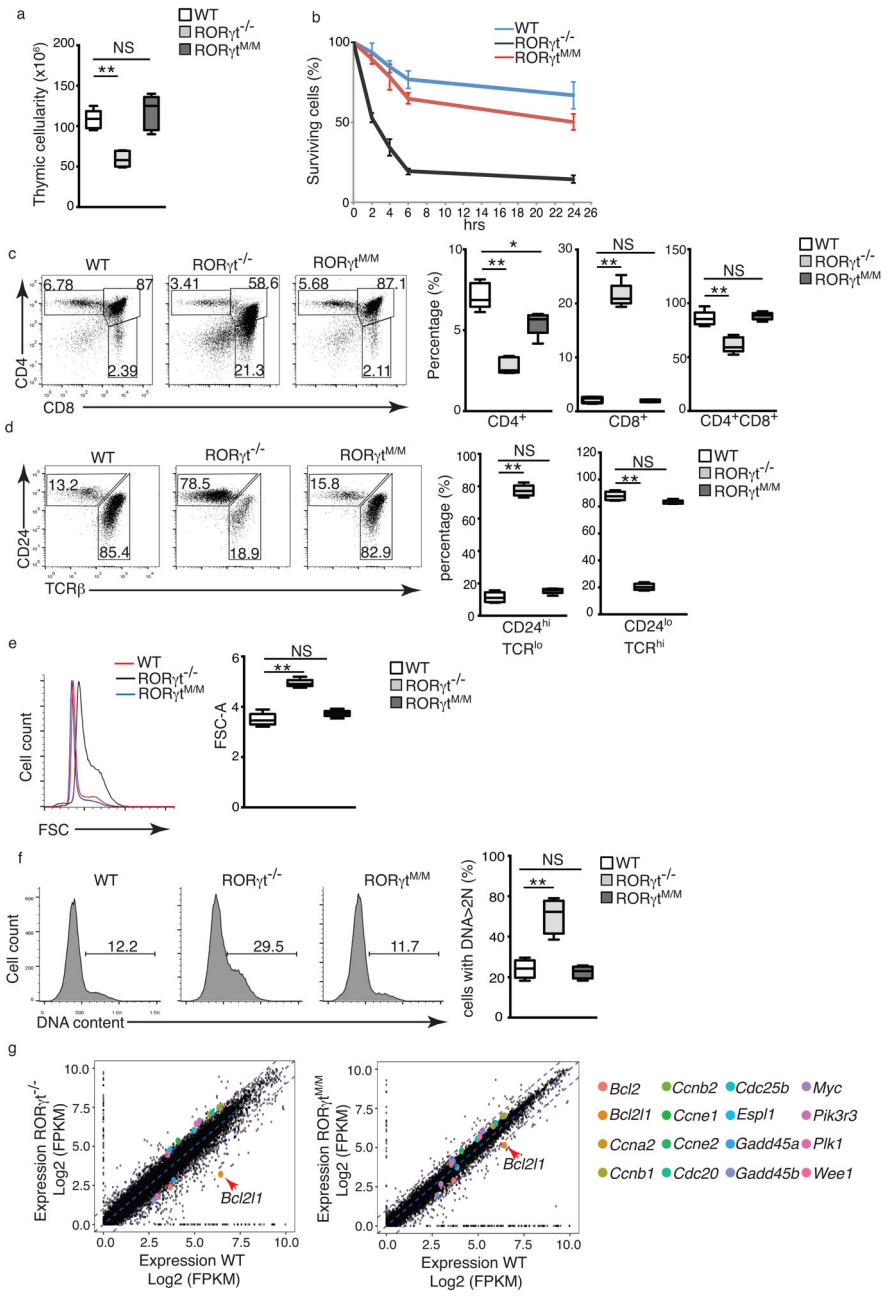

Figure 4. *RORγt*^{M} supports thymocyte development *in vivo*

(**a**) Thymic cellularity of indicated mice (n=5 per genotype). (**b**) Flow cytometer analysis of percentage of survival thymocytes stained with Annexin V and F-AAD after culturing for different times (n=3 per genotype). (**c**) Flow cytometer analysis of surface CD4 and CD8 in thymocytes. Right panel is the quantification of the percentage of indicated population of thymocytes (n=5 per genotype). (**d**) Flow cytometer analysis of CD24 and TCRβ expression for the maturity of CD8^{+} thymocytes. Right panel is the quantification of the percentage of indicated population of cells (n=5 per genotype). (**e**) Flow cytometer analysis of the forward scatter (FSC) in thymocytes of indicated mice. Right panel is the quantification of results

(n=5 per genotype). (**F**) Flow cytometer analysis of DNA content with 7-AAD in indicated thymocytes. Numbers indicate the percentage of cells with >2N of DNA. Right panel is the quantification of results (n=3 per genotype). (**g**) Comparison of gene expression profiles determined by RNA-seq between *RORγt*$^{-/-}$ and WT thymocytes (top panel) or between *RORγt*^{M} and WT thymocytes (bottom panel). Colored dots indicate selected genes. Average fragments per kilobase of transcript per million mapped reads (FRKM) values of two replicates are shown. Data in **b** are mean ± s.e.m. Central line of box-whisker plot (**a** and right panel of **c, d, e, f**) represents median and whiskers indicate extreme data points. *P < 0.05, **P < 0.01, NS non-significant (ANOVA test).Data are pooled from three experiments (**h**), are from one experiment representative of five experiments (left panel of **c,d,e and f**) or from one experiment representative of three experiments (**g** and left panel of **f**).

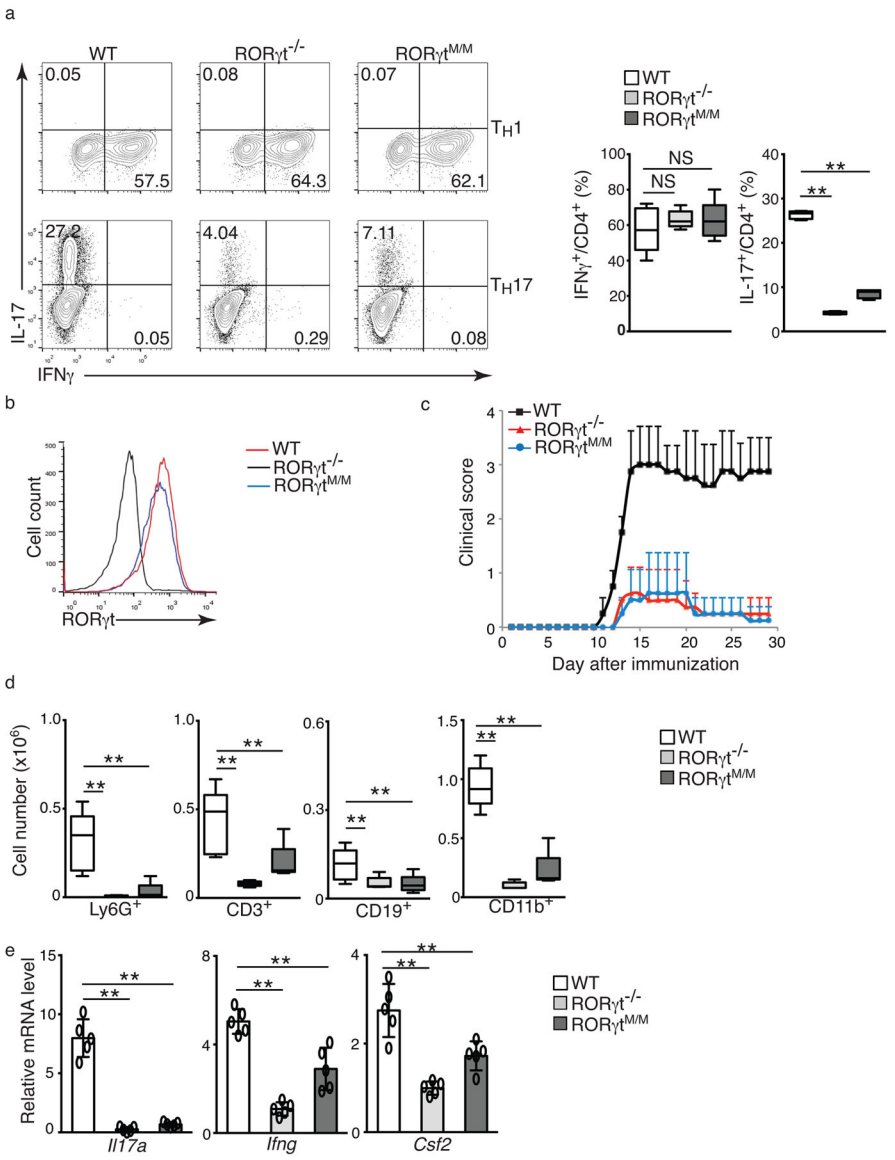

Figure 5. *RORγt*$^{M/M}$ mice have defective T_H17 differentiation

(**a**) Flow cytometer analysis of intracellular IFNγ or IL-17A in indicated naïve CD4$^+$ T cells differentiated for three day under T_H1 or T_H17 priming conditions. Right panel is the quantification of the results (n=5 per genotype). (**b**) Flow cytometer analysis of RORγt expression in T_H17 cells shown in **a**. (**c**) Mean EAE clinical score of indicated mice (female) different days after immunization with MOG_{35-55}(n=10 for WT, n=8 for RORγt$^{-/-}$ and n=13 for RORγt $^{M/M}$). (**d**) Flow cytometer analysis of surface markers for different types of CNS infiltrated lymphocytes from indicated EAE-induced mice at the peak of disease. (**e**) qPCR analysis of expression of indicated cytokines in CNS-infiltrated lymphocytes of EAE-induced mice. Data in **e** are mean ± s.e.m. Each symbol (**e**) represents an individual mouse. Central line of box-whisker plot (right panel of **a,** and **d, e**) represents median and whiskers indicate extreme data points. *P < 0.05, **P < 0.01, NS non-significant (ANOVA test).Data

are pooled from three experiments (**c**), or from one experiment representative of three experiments (**b** and left panel of **a**).

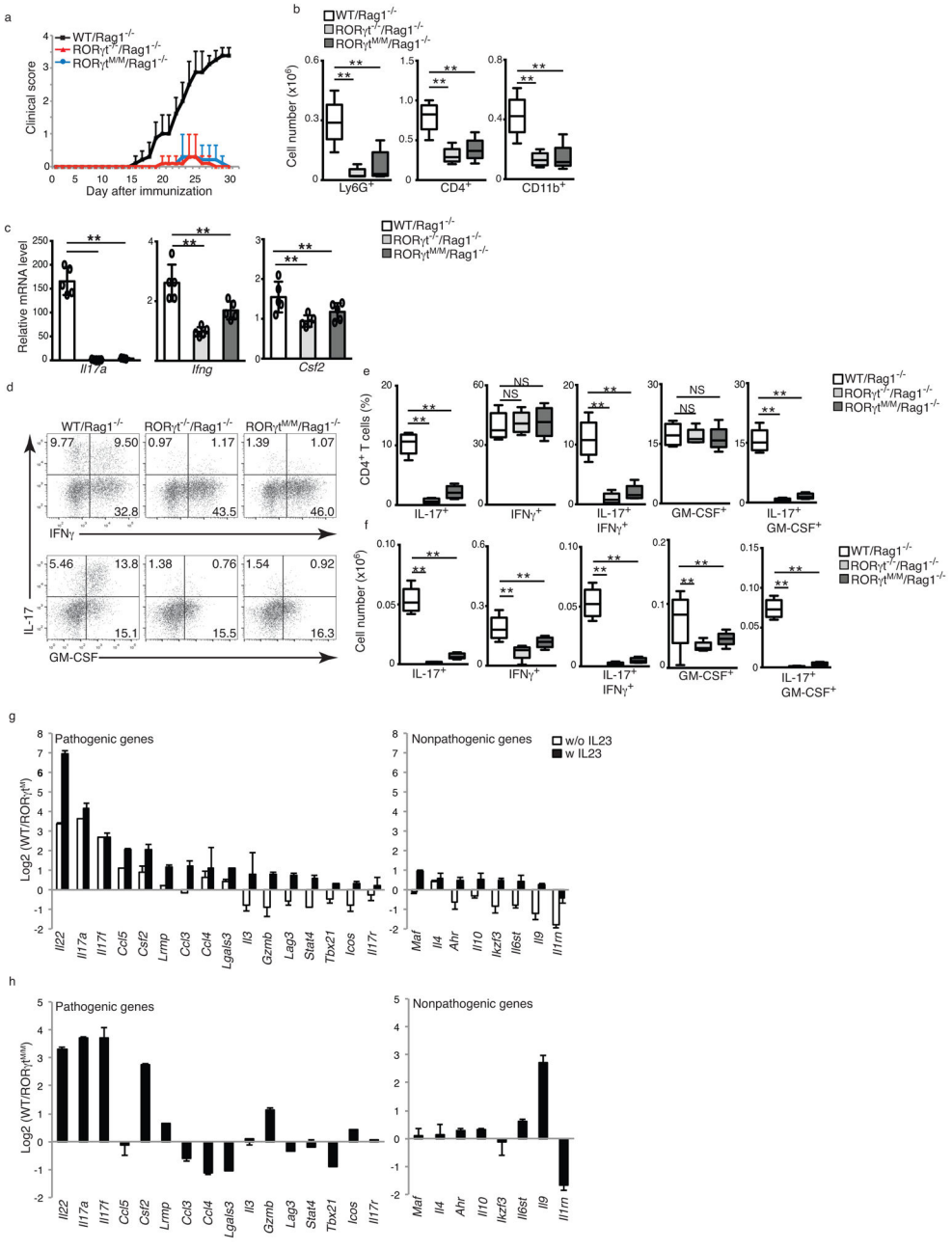

Figure 6. *ROR*$\gamma t^{M/M}$ CD4$^+$ T cells are defective in induction of EAE

(**a**) Mean EAE clinical score of *Rag1*$^{-/-}$ recipient mice (female) reconstituted with CD4$^+$ cells from indicated mice at different days after immunization with MOG_{35-55} (n=5 per genotype). (**b**) Flow cytometer analysis of indicated surface markers for different types of CNS infiltrated lymphocytes in EAE-induced mice at the peak of disease. (**c**) qPCR analysis of expression of indicated cytokines in CNS-infiltrated lymphocytes of EAE-induced mice. (**d**) Flow cytometer analysis of intracellular IFNγ and GM-CSF in CNS-infiltrated CD4$^+$ T cells from EAE-induced mice. (**e, f**) Percentage (**e**) and absolute number (**f**) of indicated CNS-infiltrated lymphocytes in EAE-induced mice. (**g**) Ratio of the expression of

pathogenic and nonpathogenic genes determined by qPCR between WT and $ROR\gamma t^{M}$ $CD4^{+}$ T cells differentiated under regular Th17 priming conditions and pathogenic Th17 priming conditions (+IL-23) for three days (n=3 per genotype). (**h**) Ratio of the expression of pathogenic and nonpathogenic genes determined by qPCR between WT and $ROR\gamma t^{MM}$ $CD4^{+}$ T cells obtained from EAE-induced mice (n=3 per genotype). Data **c** are mean ± s.e.m. $^{**}P < 0.01$, NS non-significant (ANOVA test). Each symbol (**c**) represents an individual mouse. Central line of box-whisker plot (**b, e** and **f**) represents median and whiskers indicate extreme data points. Data are pooled from three experiments (**a,b,c,e,f,g and h**), or from one experiment representative of three experiments (**d**).

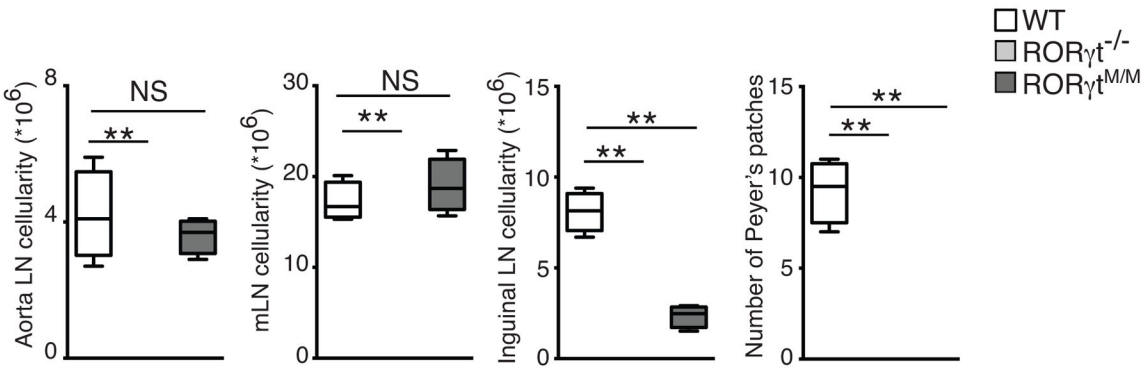

Figure 7. *ROR*$\gamma t^{M/M}$ mice develop lymph nodes, but not Peyer's patches

Cellularity of aorta, mesenteric, and inguinal lymph nodes and total number of Peyer's patches in indicated mice (n=5 per genotype). Central line of box-whisker plot represents median and whiskers indicate extreme data points. $^{**}P < 0.01$, NS non-significant (ANOVA test). Data are pooled from 5 mice.

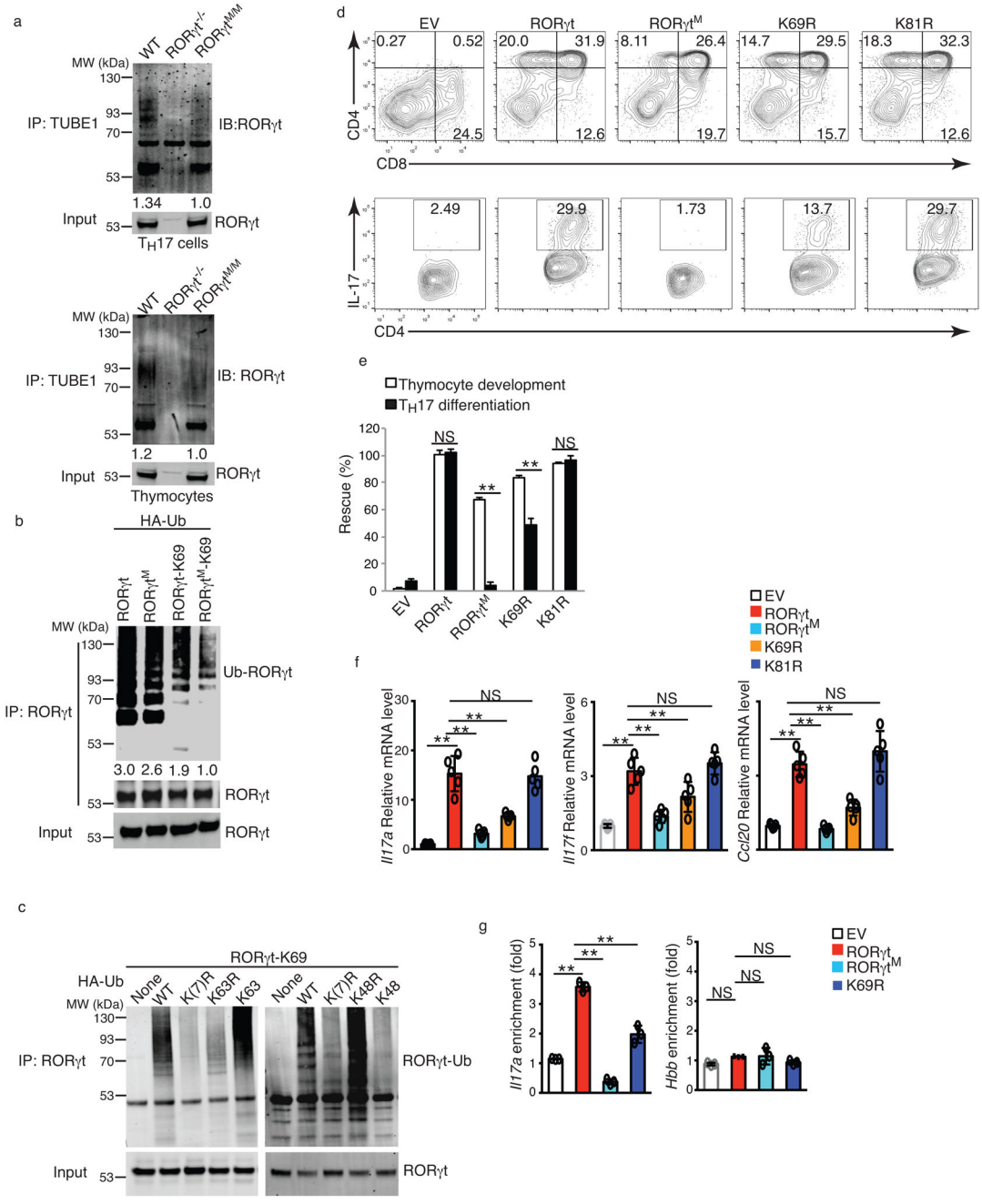

Figure 8. RORγt^{M} interferes with the ubiquitination of RORγt at lysine 69

(**a**) Western blot analysis of *RORγt* in TUBE1-enriched ubiquitinated proteins from differentiated T_H17 cells (left panel) or thymocytes (right panel). (**b**) Western blot analysis of ubiquitinated RORγt (Ub-RORγt) in HEK 293T cells expressing RORγt or RORγt-K69, together with HA-tagged ubiquitin for 48 hrs. (**c**) Western analysis of Ub-RORγt in HEK 293T cells expressing RORγt-K69, together with HA-tagged WT or mutated ubiquitin. (**d**) Flow cytometer analysis of CD4 and CD8 in *ex vivo* development of thymocytes (top panel) or IL-17A^{+} cells in T_H17 differentiation for three days in *RORγt*$^{-/-}$ thymocytes or CD4^{+}

cells retrovirally expressing indicated RORγt mutants. (**e**) Quantification of results shown in **d.** (**f**) qPCR analysis of mRNA levels of indicated genes in Th17 cells shown in **e**. (**g**) ChIP analysis of indicated RORγt binding to IL-17 promoter in *RORγt*$^{-/-}$ CD4^{+} T cells retrovirally expressing various RORγt and differentiated under T_H17 priming conditions for three days. Hemoglobin gene (*Hbb*) locus is a control. Data in **e,f,g** are mean ± s.e.m. $^{**}P < 0.01$, NS non-significant (ANOVA test). Each symbol (**f, g**) represents an individual experiment. Data are pooled from three experiments (**e, g**), from five experiments (**f**), or from one experiment representative of three experiments (**a,b,c** and **d**). Full length gel imagines are available in supplementary figure 8.

Table 1

Visualization of presence and absence of aorta, mesenteric, and inguinal lymph nodes in indicated mice (n=10 per genotype). Data are pooled from 10 mice.

Mouse strain	Aorta LN	Messenteric LN	Inguinal LN	Peyer's patches
WT	+	+	+	+
RORγt$^{-/-}$	−	−	−	−
RORγt$^{M/M}$	+	+	+	−